

# On the long and short nulls, modes and interpulse emission of radio pulsar B1944+17

Isabel M. Kloumann<sup>1</sup> & Joanna M. Rankin<sup>2,1</sup>

<sup>1</sup>*Physics Department, University of Vermont, Burlington, VT 05405\**

<sup>2</sup>*Sterrenkundig Instituut ‘Anton Pannekoek’, University of Amsterdam, NL-1098 XH*

Accepted 2009 month day. Received 2009 month day; in original form 2009 month day

## ABSTRACT

We present a single pulse study of pulsar B1944+17, whose non-random nulls dominate nearly 70% of its pulses and usually occur at mode boundaries. When not in the null state, this pulsar displays four bright modes of emission, three of which exhibit drifting subpulses. B1944+17 displays a weak interpulse whose position relative to the main pulse ( $\Delta\phi_{IP-MP}$ ) we find to be frequency independent. Its emission is nearly 100% polarized, its polarization-angle traverse is very shallow and opposite in direction to that of the main pulse, and it nulls approximately two-thirds of the time. Geometric modeling indicates that this pulsar is a nearly aligned rotator whose  $\alpha$  value is hardly  $2^\circ$ —*i.e.*, its magnetic axis is so closely aligned with its rotation axis that its sightline orbit remains within its conal beam. The star’s nulls appear to be of two distinct types: those with lengths less than about 8 rotation periods appear to be *pseudonulls*—that is, produced by “empty” sightline traverses through the conal beam system; whereas the longer nulls appear to represent actual cessations of the pulsar’s emission engine.

**Key words:** miscellaneous –null– interpulse – emission modes – methods: — data analysis – pulsars: general, individual (B1944+17)

## 1 INTRODUCTION

Pulsar B1944+17 was discovered in August 1969 at the Moulton Radio Observatory. This 440-ms pulsar attracted attention thereafter because of its long null intervals, (Backer, 1970). Remarkably, it nulls some 70% of the time and exhibits null lengths ranging between 1 and 300 stellar-rotation periods (hereafter  $P_1$ ). In 1986 Deich *et al.* (hereafter DCHR) investigated B1944+17’s nulling behavior based on the received notion that its nulls represented “turn offs” of the pulsar emission mechanism. Thus they were concerned with the time scales of the cessations and resumptions of emission. While some pulsars, indeed, do appear to “turn off” for extended intervals—notably B1931+24 (Kramer *et al.* 2006)—there is a growing body of evidence that many nulls do not represent a shutdown of a pulsar’s emission engine.

Specifically, we now know that conal beams are comprised of rotating “carousels” of subbeams, and in certain situations nulls (or what might better be called *pseudonulls*) represent “empty” sightline passes through a subbeam carousel. Such carousel “action” was first demonstrated in pulsar B0943+10 (*e.g.*, Deshpande &

Rankin 1999, 2001; Suleymanova & Rankin 2009), and then *pseudonulling* was identified in pulsars B2303+30 (Redman *et al.* 2005; B0834+06 (Rankin & Wright 2007) and J1819+1305 (Rankin & Wright 2008). Furthermore, periodicities clearly associated with nulling were discovered in pulsar B1133+16 by Herfindal & Rankin (2007) and then subsequently in a number of other stars (Herfindal & Rankin 2009; hereafter HR07/09), and such periodicities are almost certainly carousel related.

There remain a small number of pulsars, however—B1944+17 prominent among them—whose observed nulling effects are not easily ascribed to either mechanism. That is, neither emission cessations, marked by partial nulls with near instantaneous decay times, nor “empty” sightline traverses through a rotating subbeam carousel, marked by null periodicities, provide any clear explanation.

Pulsar B1944+17 exhibits a complex combination of behaviors including both very short and very long nulls. In addition, DCHR identified what appeared to be several distinct emission modes, denoted A–D. And furthermore, Hankins & Fowler (1986; hereafter HF86) discovered that B1944+17 has a weak interpulse that nulls in synchrony with its main-pulse region (hereafter IP/MP). Synchronous nulling indicates, remarkably, that whatever mechanism is responsible for MP nulling is also controlling the IP emission.

\* Isabel.Kloumann@uvm.edu; Joanna.Rankin@uvm.edu

The presence of both MP and IP emission raises vexing questions about the overall emission geometry of the star. Several analyses of pulsar geometry (*e.g.*, Lyne & Manchester 1988; Rankin 1993a,b, hereafter R93a,b) have mentioned B1944+17, but as for virtually all such pulsars,<sup>1</sup> no credible model of its overall MP-IP emission geometry has yet been articulated. In short, neither an “opposite pole” nor “single pole” IP geometry provides an obvious solution, so among the various other issues, this basic question is still open for B1944+17.

When not in the null state, MP pulse sequences (hereafter PSs) exhibit four modes of emission, three of which are well defined drift modes. Burst lengths are as large as 100 pulses, indicating a non-random null-burst distribution. The strict organization of the principle drift mode (Mode A, to be defined below) is in stark contrast with the disorganized non-drifting burst mode (Mode D) as well as the pulsar’s preponderance of null pulses.

The rich variety of PS effects exhibited by this pulsar complicates its analysis, as well as any effort at modeling its many phenomena. While B1944+17 exhibits so many different identifiable behaviors (organized drifting, nearly “chaotic” subpulse behavior, bright emission, short nulls, long nulls, etc.), what makes the star so compelling is that in any time interval of reasonable length, ( $\sim 2000 P_1$ ), one *will* see each of these behaviors. This consistency indicates that the processes that produce such variable emission patterns are in some way repeating themselves.

This paper reports a new synthetic study of pulsar B1944+17. We have conducted long, high quality polarimetric observations using the upgraded Arecibo telescope at both meter and decimeter wavelengths, carefully analyzed the star’s emission and nulls on a PS basis, and reconsidered the emission geometry of its MP and IP. §2 describes the observations, §3 details aspects of our analyses, §4 builds a geometrical model, and §5 presents our thorough null analysis. §6 then provides a summary and discussion of our results.

## 2 OBSERVATIONS

The observations used in our analyses were made using the 305-m Arecibo Telescope in Puerto Rico. The 327-MHz (P band) and 1400-MHz (L band) polarized PSs were acquired using the upgraded instrument together with its Gregorian feed system and Wideband Arecibo Pulsar Processor (WAPP<sup>2</sup>) on 2006 August 19 and 2008 March 15, consisting of 7038 and 5470 pulses, respectively, see Table 1. The auto- and cross-correlations of the channel voltages were three-level sampled and produced by receivers connected to orthogonal linearly polarized feeds (but with a circular hybrid at P band). Upon Fourier transforming, sufficient channels were synthesized across a 25-MHz (100-MHz at L band) bandpass, providing resolutions of approximately 1 milliperiod of longitude. The Stokes parameters have been corrected for dispersion, interstellar Faraday rotation, and

<sup>1</sup> Until very recently that is; see Weltevrede & Wright (2009) and Keith *et al.* (2010).

<sup>2</sup> <http://www.naic.edu/~wapp>

**Table 1.** Observations

Band	MJD	BW (MHz)	Resolution ( $^{\circ}$ )	Pulses (#)
P band	53966	25	0.31	7038
L band	54540	300	0.21	5470

various instrumental polarization effects. At L band, four 100-MHz channels were observed with centers at 1170, 1420, 1520, and 1620 MHz. Both of the observations encountered virtually no interference (hereafter RFI), except for the 1620 MHz channel at L band which was disregarded. At L band, the lower three 100-MHz bands were appropriately delayed and added together to give a 300-MHz effective bandwidth. The PPAs of the two observations are approximately absolute in that they have been corrected for both ionospheric and interstellar Faraday rotation.

## 3 ANALYSES

Figure 1 presents the polarized profiles and polarization-angle (hereafter PPA) histograms of pulsar B1944+17 at both 327 and 1400 MHz. While these profiles are familiar, it is useful to inspect them in detail. Notice that the half-power or equivalent width of the star’s roughly symmetrical profile increases greatly at higher frequencies; whereas the more than  $\pm 25^{\circ}$ -longitude interval over which significant emission is observed changes hardly at all. The PPAs also reiterate this circumstance clearly; the discontinuous orthogonal polarization mode (hereafter OPM) extends over the full  $\gtrsim 50^{\circ}$  width of the profiles, whereas the more prominent OPM occupies a more restricted longitude range at the lower frequency. As the PPAs are nearly absolute and the two OPMs lie conveniently in the upper and lower halves of the PPA panel, we will refer to them as the “positive” and “negative” polarization mode, respectively.<sup>3</sup> The star’s profile has been classified previously (R93a,b) as belonging to the conal triple (cT) class; looking more closely, however, at the overall L-band form, it would be more accurate to regard it as exhibiting a hybrid cT and conal quadruple (cQ) behaviour. This said, the two profiles are so different in form that it is not easy to see how to align them. Rather, we have used the structures of stationary modulation on the leading and trailing edges of the PSs, and we note that this tends to align the profile edges but not the peaks. We will come back to considering how these characteristics should be interpreted below.

<sup>3</sup> Interestingly, Hobbs *et al.*’s (2005) determination of B1944+17’s proper-motion direction of  $174^{\circ} \pm 29^{\circ}$  gives the possibility that the fiducial PPA is aligned with the star’s velocity vector in the sense of Johnston *et al.* (2006) and Rankin (2007). Of course, even if so the double ambiguity of supernova “kick” orientation and OPM identification makes interpretation impossible at this time.

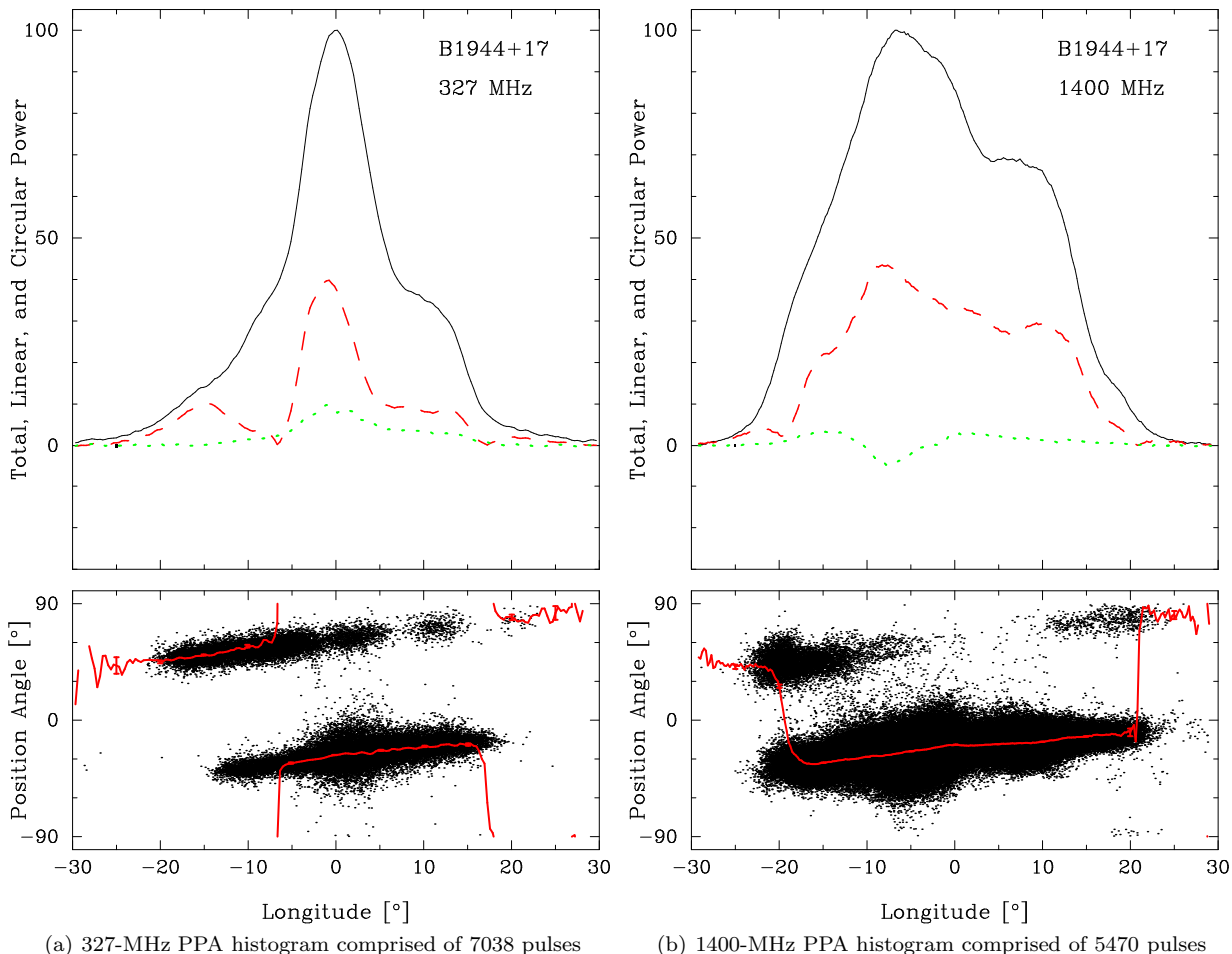


**Figure 1.** The two panels display the total power (Stokes  $I$ ), total linear polarization ( $L [= \sqrt{Q^2 + U^2}]$ ; dashed red) and circular polarization (Stokes  $V$ , defined as left – right-hand; dotted green) (upper), and the polarization angle ( $PPA [= \frac{1}{2} \tan^{-1}(U/Q)]$ ) (lower). Individual samples that exceed an appropriate  $>2$  sigma threshold appear as dots with the average PPA (red curve) overplotted. The tiny black box at the left of the upper panel gives the resolution and a deflection corresponding to three off-pulse noise standard deviations. The PPAs are approximately absolute, such that the discontinuous regions of OPM emission at positive and negative PPAs correspond to each other. Note that the P and L-band profiles each extend **more than**  $\pm 25^\circ$  and that the lower frequency profile has an unusually narrow equivalent width relative to its higher frequency counterpart.

### 3.1 Non-Random Null Distribution

In our observations, B1944+17 nulls about 2/3 of the time, somewhat higher than the 60% value given by DCHR, but closer to null percentage reported by Rankin, (1986). The majority of these null pulses can readily be distinguished from the bursts; however, there is a small portion of weak pulses that are difficult to identify as either nulls or pulses. Interestingly, the distinction between nulls and pulses is easier to define at L band, as can be seen in the respective null histograms of Fig. 2.

Given that the nulls and pulses cannot be fully distinguished, we can choose an intensity threshold that will be conservative and reliable either in selecting pulses or nulls, but not both. In Fig. 2, we have taken the latter option—that is, using low thresholds that will tend to slightly underestimate the null population. Then, using this conservative discriminator of nulls, we have computed the burst- and null-length histograms in Figure 3. These show that 1-pulse bursts and nulls have the highest frequency, but we see that

very long bursts and nulls also occur. In the 7000-pulse 327-MHz observation, for instance, a small number of bursts of 40-50  $P_1$  and two of 80-90  $P_1$  were encountered alongside the more frequent long nulls ranging up to 300  $P_1$ . Even qualitatively we immediately see that the nulls in B1944+17 are distributed within the PS in a very non-random manner.

Recent investigations into pulsar nulling have raised two important new questions about their distributions: a) whether they are randomly distributed (*e.g.*, Redman & Rankin 2009; Rankin & Wright 2007); and b) whether they are periodic (HR07/09). With such a large null fraction, one would expect to see few long sequences in any given observation. The tendency of B1944+17’s bursts and nulls to clump into sequences of roughly 20-100 pulses immediately indicates a non-random distribution. Application of the above RUNS<sup>4</sup> test to our observations, namely burst and null se-

<sup>4</sup> The RUNS test for detecting non-randomness returns a value greater than 1.96 in absolute value if the data is non-randomly sequenced; see Redman & Rankin (2009).

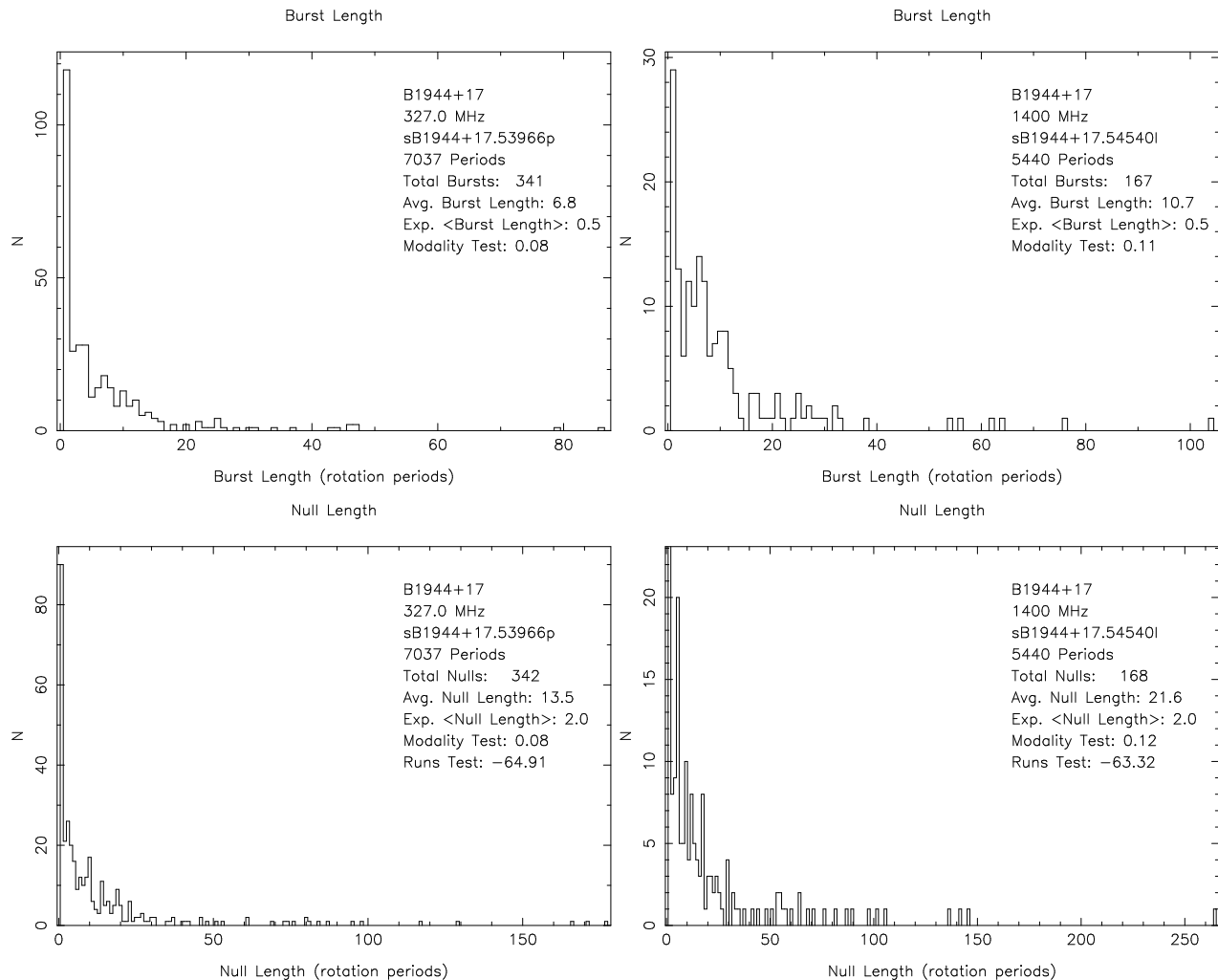


**Figure 3.** Burst- and null-length histograms corresponding to the P- and L-band observations and thresholds in Figure 2. These distributions show unsurprisingly that burst and null lengths of a single rotation period are highly favored; however, we also see that bursts can last up to approximately  $90 P_1$  and nulls up to three times this! Thus, in the language of the Runs Test, the nulls occur non-randomly in the PS by virtue of being “undermixed” (see text). Note that the P-band observation included nulls up to  $300 P_1$ ; however the null histogram has been truncated down to 180, so as to resolve detail in the short null distribution.

quences, returns values  $\lesssim -60$ , verifying this conclusion of a non-random “undermixing”. Regarding null periodicity, we find only a suggestion in our observations of a very long periodicity—far too long in relation to their total length for it to be significant.

Thus the bursts and nulls of B1944+17 can be regarded as falling into two categories: a) short bursts or nulls of some  $1-7 P_1$  that show a roughly random distribution, and b) medium to long bursts or nulls ( $>20 P_1$ ) that can occasionally persist for several hundred pulses and are patently non-random. We will elaborate further on this distinction in §5.

### 3.2 Modes of emission

We here investigate the properties of the four modes identified by DCHR. Following their convention, we refer to the three drift modes as A-C, and the final burst mode as “D”.

The defining characteristics of modes A-D are the same at both P and L band, as are their frequencies of occurrence.

The four modes can be readily distinguished by eye due to their unique subpulse structures and intensities, as shown in Figure 4. The transitions between modes occur on a time scale of less than one pulse—*i.e.*, there are typically no observable “transitions” between modes.<sup>5</sup> We find that within a sequence of  $10^3$  pulses there is a high probability of finding at least one occurrence of each mode. It is interesting that this pulsar, which displays an almost overwhelming variety of behaviors, is quite reliable in how often it does so.

As seen in the colour polarization display of Fig. 4, the star’s mode changes are usually punctuated by nulls, though there are some combinations of mode changes that characteristically occur adjacent to one another.

<sup>5</sup> With two notable exceptions, discussed in the null section.

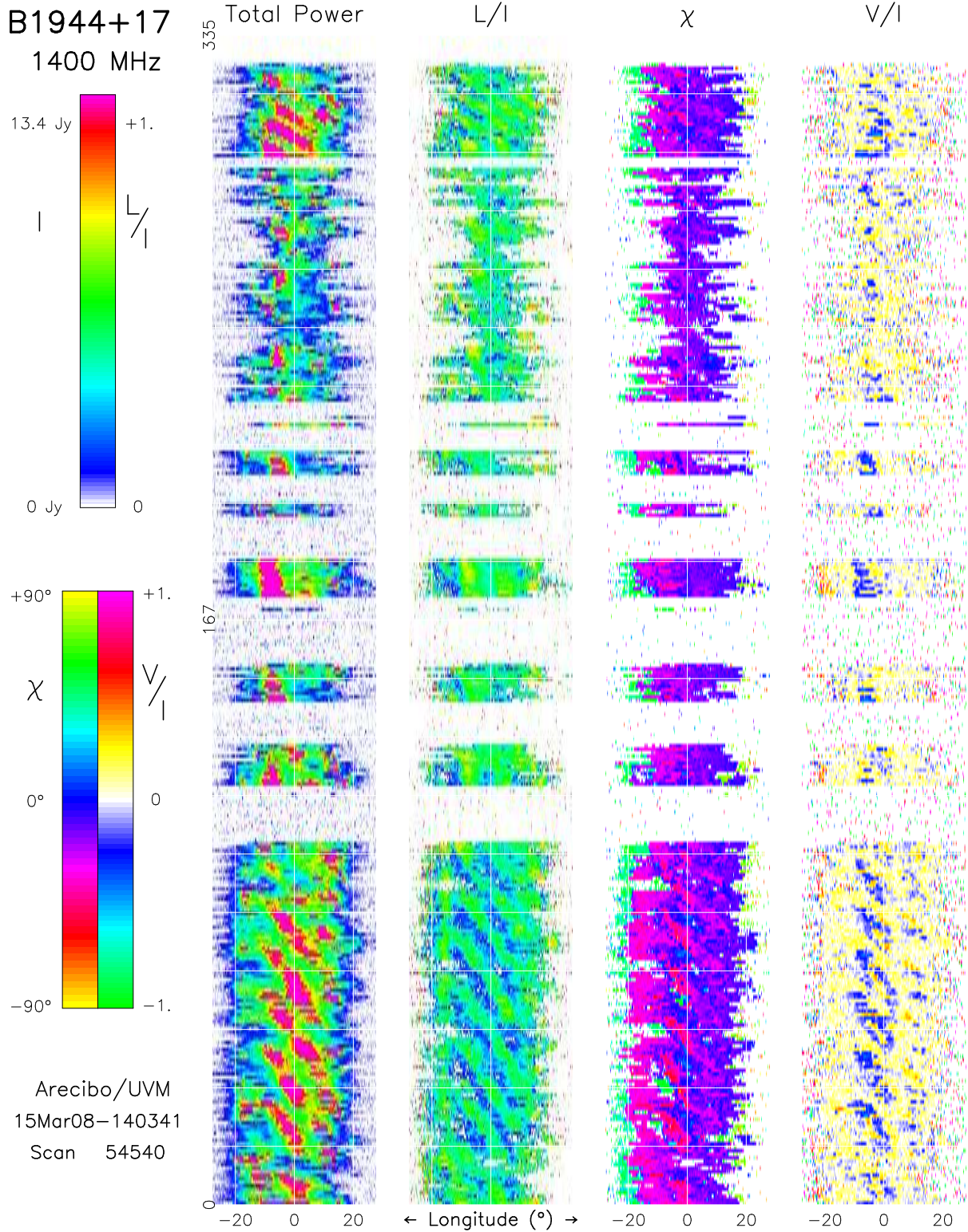


**Figure 4.** Pulse-sequence polarization display showing several of the pulsar’s PS behaviors, with reordered mode sequences. The bright and ordered subpulses of mode A begin at pulse 1 and last for 110 periods. Mode A is succeeded by mode C, separated by a null. Mode C is characterized by roughly stationary subpulses and a quasi-periodic cycle of short bursts and nulls. The next 100 pulses (190-290) are mode D, the weakest and least structured of the star’s modes. Note the weak evidence of subpulse structure. Mode D is succeeded by a bright and very well defined mode B, separated by a three-period null. The total power  $I$ , fractional linear  $L/I$ , PPA  $\chi$ , and fractional circular polarization  $V/I$  are colour-coded in each of four columns according to their respective scales at the left of the diagram. Both the background noise level and interference level of this observation are exceptionally low with the former effectively disappearing into the lowest intensity white portion of the  $I$  color scale.

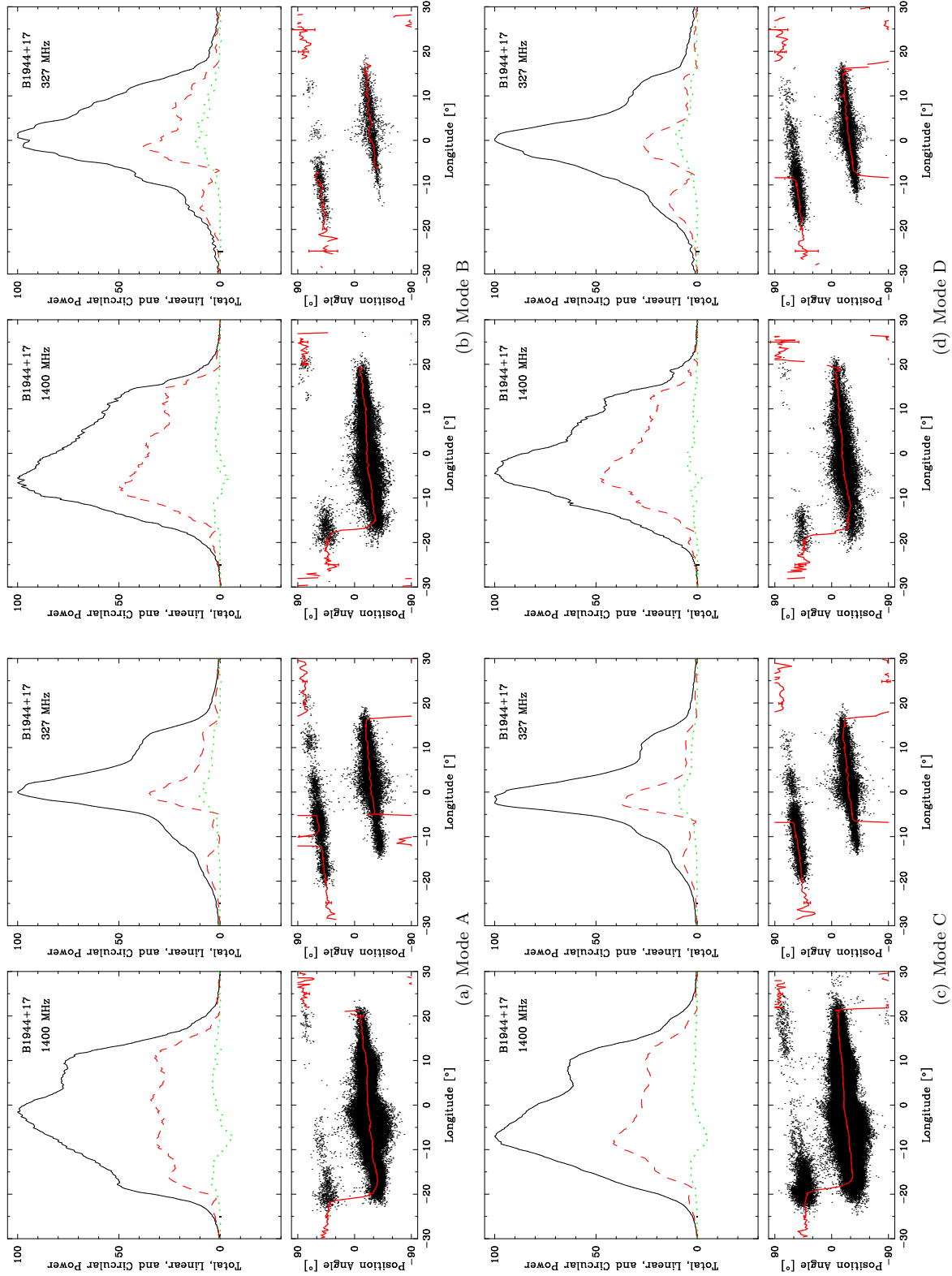


**Figure 5.** Partial polarized profiles after Fig. 1 for the four modes at L and P band. The base width within which there is measurable emission is roughly constant in all the modes at both frequencies. There is, however, significant variation in the FWHMs of the various modes at the two different bands. Most notable is the narrowing of the FWHM at P band, clearly displayed in every mode. Also, at L band the FWHMs of modes A and C are broader than those of modes B and D. Conversely, at P band the FWHMs of modes B and D are broader than those of modes A and C. Numerical values for modal properties are summarized in Table 2.

**Table 2.** Emission Modes of B1944+17

Mode	Frequency Band	$P_2$ (°)	$P_3$ ( $P_1$ )	Percentage of total pulses	Number of Bursts	Number of Drift Bands	Average Burst Length	FWHM
A	L band	$12.2 \pm 1.0$	$13.9 \pm 0.6$	$8.4 \pm 0.05$	14	25	32.5	29
	P band	$13.5 \pm 1.0$	$13.5 \pm 1.1$	$6.4 \pm 0.05$	11	33	41.1	10
B	L band	$11.0 \pm 1.6$	$6.5 \pm 1.7$	$3.3 \pm 0.05$	8	9	22.0	26
	P band	$8.5 \pm 1.7$	$5.6 \pm 1.8$	$1.4 \pm 0.05$	8	10	11.9	18
C	L band	$12.1 \pm 1.1$	n/a	$17.9 \pm 0.05$	118	n/a	8.1	28
	P band	$13.6 \pm 0.9$	n/a	$8.8 \pm 0.05$	78	n/a	8.0	9
D	L band	n/a	n/a	$4.4 \pm 0.05$	22	n/a	11.0	21
	P band	n/a	n/a	$20.6 \pm 0.05$	119	n/a	12.1	12

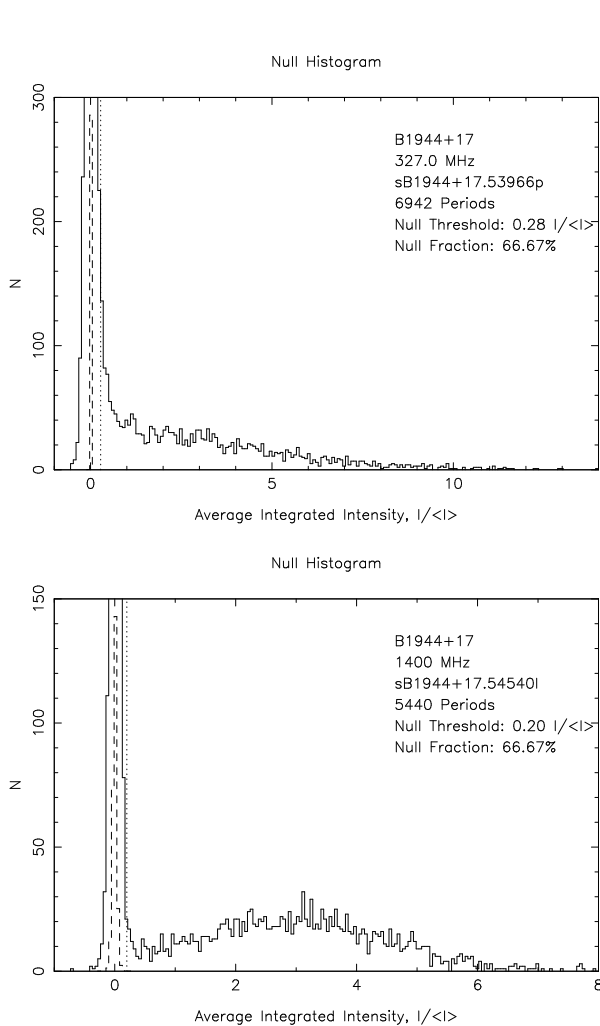


**Figure 2.** Null histograms for B1944+17 at P (top) and L (bottom) bands. The histogram peaks (at 1110 and 980) corresponding to the large null fractions have been truncated in order to better show the pulse-amplitude distribution. Despite the high S/N, the star’s null- and pulse-energy distributions overlap, so that the nulls and pulses cannot be fully distinguished, though this difficulty is more severe at P band than at L band. Plausible, conservative thresholds (shown by dotted vertical lines) of 0.28 and 0.20  $\langle I \rangle$ , respectively, indicate that some 2/3 of the pulses are nulls or pseudonulls.

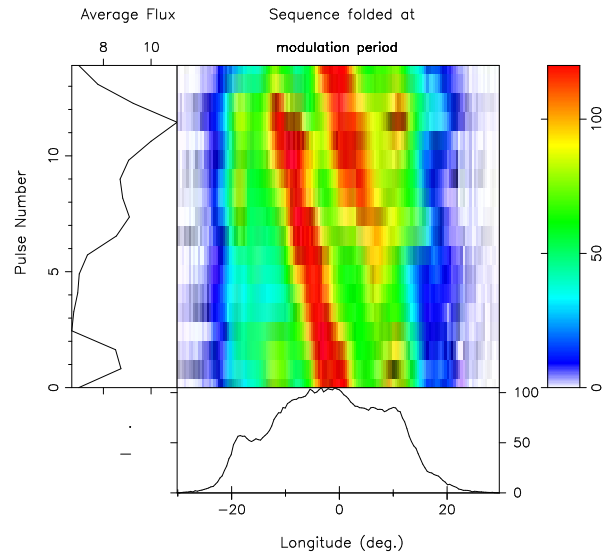


**Figure 6.** A  $50\text{-}P_1$  mode-A interval at L band. The PS has been folded at a  $P_3$  of  $14 P_1$ . The fold length was chosen to demonstrate that the peripheral conal outliers, seen here mainly on the leading edge of the pulse window, fluctuate with a period equal to mode A’s  $P_3$ .

### 3.2.1 Modal distinctions in subpulse structure

As modes A and B exhibit subpulse drifting, they can best be characterized by their  $P_2$  and  $P_3$  values, where  $P_2$  is defined as the separation of subpulses within a period, and  $P_3$  is the separation between drift bands at a fixed pulse phase. Mode C characteristically displays an organized yet stationary subpulse structure. Lastly, we classify those PSs which show no organized subpulse structure as mode D; it is worth noting that mode D is significantly weaker than the others.

Table 2 gives  $P_2$  and  $P_3$  values for modes A, B, and C. The A mode is characterized by prominent intervals of remarkably precise drifting subpulses—which is paradoxical considering the star’s otherwise unpredictable and discontinuous behavior. Mode A is unique in its regularity and is marked by its negatively-drifting bands with a roughly  $14\text{-}P_1 P_3$ . This  $14\text{-}P_1 P_3$  feature can be seen in an lrf of a PS that includes all the modes, indicating its dominance (Weltevrede *et al.* 2006, 2007). Two bright, central subpulses are usually seen in mode A.

At L band, weak subpulses on the outer edges of the

profile turn on and off with a period that is comparable to mode A's  $P_3$ ; see Figure 6. Mode A always appears in bursts having durations of more than 15 periods; however, usually these bursts are even longer, typically some 60 – 100  $P_1$ —and, remarkably, these A-mode intervals are very rarely interrupted by nulls.

The drifting subpulses of mode B are visibly less ordered than those of mode A; however they are clearly structured and negatively-drifting.  $P_3$  is approximately half that of mode A at both L and P band; although due to its irregularities these values cannot be measured with the same degree of precision as for mode A. The B mode characteristic persists for less than 25  $P_1$ .

The third “drift” mode, C, displays three roughly stationary subpulse drift bands ( $P_3/P_2 \approx 0$ ), with the components’ relative intensities being variable. Mode C manifests itself in a complex variety of ways: most often the intensities of the three components are approximately equal to each another; see Fig. 4. However, one or two of the components intermittently either turns off or notably weakens relative to the other two; every combination of the three constituent components was observed. The  $P_2$  value for mode C is similar to that of mode A, taking into account the presence or absence of its three constituent features.

It is possible that the nearly vertical drift bands in mode C result from a near stoppage of carousel rotation; it is also possible that this is an effect of aliasing. Because of the other similarities between modes A and C, it is likely that this “stopping” happens during what is otherwise known as mode A. The difference between modes A and C is therefore only the carousel motion, not the fundamental subpulse structure. This dynamic accounts for the varying number of subpulses observed in mode C. In mode A, as the subpulses drift across the pulse window, anywhere between 1 and 3 may be seen depending on the modulation phase—*i.e.*, see Fig. 6.

In mode C short bursts and nulls alternate quasiperiodically with each burst or null lasting some 10  $P_1$  or so, and switching back and forth up to 10 times. The length of these segments is very comparable to the  $P_3$  of mode A.

Deich *et al.* first referred to mode D as “chaotic”—that is, displaying little perceptible order in its subpulses. Our investigation has uncovered a slightly different story for mode D. The mode-D emission does not usually span the entire pulse window, see Fig. 4. While its sparse subpulses are overshadowed by the bright and ordered ones of modes A, B and C, they appear to consistently have an underlying characteristic structure. Mode D’s brightest subpulses appear approximately every 5–10  $P_1$  on the leading edge of its substantially narrower emission window. This withdrawal of emission in the profile wings is unique to mode D.

### 3.2.2 Modal distinctions in total and linear power distributions

Figure 5 gives partial polarized profiles for each of the four modes at L and P band. The profiles have different total power and total linear forms in the different modes. Most evident are their different modal widths in each of the bands.

Mode A has the broadest modal profiles; see Figure 5(a). Its L-band profile displays a nearly uniform distribution of linear power across the pulse window, showing only

small dips that correspond to the subpulse separation. Its leading edge is marked by a distinct shoulder at both L and P band, also visible in the linear power, a feature hardly seen in any of the other modes at L band. The bright central subpulses in mode A display a linear power distribution that indicates there are in fact two distinct features that lead the central peak. They can be identified at both bands, though the second one is weaker at P band, nevertheless distinguishing itself as a unique feature. Also in both bands, the trailing subpulse features are brighter and more clearly defined than the leading ones.

The mode-B profiles display a slightly narrower FWHM than in mode A; see Table 2 and Fig. 2. The leading feature in mode A’s profile is clearly visible in mode B at P band but is very weak at L band; see Figure 5(b). At L band, the central peak of mode B occurs  $\sim 6^\circ$  earlier than in mode A; at P band the peaks of the two modes occur in the same location. The trailing feature in mode B is poorly defined, however this is likely due to the dense drift bands blurring the intensity distribution between the leading and trailing features, rather than a decrease of subpulse intensity.

Mode C displays a FWHM width nearly as broad as that of mode A; see Table 2. There is more evidence for the leading feature in the linear power distribution of mode C than in mode B. As in mode B, the central peak in mode C at L band is shifted  $6^\circ$  earlier relative to the peak in mode A, whereas at P band they occur at the same longitude. The trailing component is very well defined in mode C in the profiles of both bands.

Mode D displays a significantly narrower profile at L band compared to the other modes. As in mode B, its leading component is very poorly defined at L band, though there is some evidence for it in the linear power distribution. At L band, the central peak of mode D is shifted approximately  $4^\circ$  compared to that of mode A. At L band, the trailing feature is slightly more distinct in mode D than in mode B, though it remains weak. The trailing feature at P band is well defined.

### 3.2.3 Mode changes

Mode changes are often punctuated by nulls, with two distinct exceptions: First, a small proportion of mode changes are characteristically not interrupted by a null. We find that mode D often precedes modes A and B and sometimes succeeds mode B continuously. Second, nulls do not necessarily result in mode changes. Mode C (discussed below) characteristically displays a pattern in which the emission turns on and off in segments of short 10–15  $P_1$  bursts and nulls. Short nulls are associated both with this mode-C emission pattern as well as with transitions between modes A, B, C and D.

## 3.3 Main Pulse – Interpulse Relationship

We have used the conservative thresholds of 0.28 and 0.20  $< I >$  to build partial P- and L-band PSs of the pulses and nulls. Full period polarization profiles corresponding to the pulses (not the nulls) are shown in Figure 7 and are similar to the MP profiles in Fig. 1 except that Stokes  $I$ ,  $L$  and  $V$  are replotted at 50X scale to reveal the structure of the



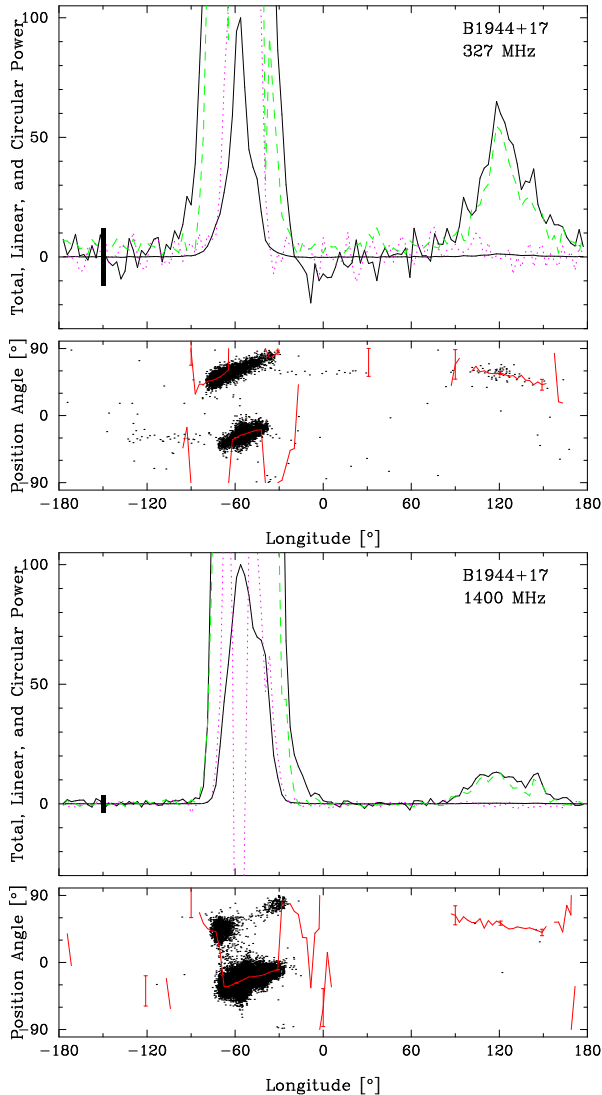


**Figure 7.** Full period polarization profiles (after Fig. 1) of the P- (upper) and L-band (lower) partial PSs containing the pulses (falling above the thresholds in Fig. 2, numbering 2403 and 1803 pulses, respectively), not the nulls. Here, the total power is shown at full scale and then Stokes  $I$ ,  $L$  and  $V$  are replotted at 50X scale in order to reveal the structure of the interpulse; otherwise the displays are identical to those in Fig. 1. Only 128 longitude bins were used across the full profile so as to maximize the S/N of each sample. Note the virtually complete IP linear polarization and the similarity in half-power widths between the IPs in the two bands. Note also that the centers of the PPA traverses of the IP and MP (positive OPMs) both fall at about  $+60^\circ$  and have opposite slopes.

IP. Here we see clearly for the first time that the B1944+17 IP is almost fully linearly polarized (and has negligible circular), that its half-power width is very comparable at the two frequencies, and that its IP PPA traverse is centered at virtually the same angle as the MP positive-mode, but with a negative slope. In the 327-MHz profile, the discrete PPA dots under the IP profile show that some IP samples are strong enough to define their linear polarization; thus the IP is not uniformly weak, but exhibits a range of intensities. We can also confirm that the IP-to-MP intensity

ratio ( $S_{IP}/S_{MP}$ ) decreases with frequency, being about 1% at P and some 0.2% at L band. HF86 reported values of about 3% at 430 MHz and 0.3% at L band. Notably, they found that most pulsars with IPs show a similar decrease as frequency increases. More perplexing was HF86’s finding that the MP-to-IP spacing ( $\Delta\phi_{IP-MP}$ ) decreases by some  $10^\circ$  between P and L band, and given the drastic changes in MP form it is not fully clear how such a change could even be consistently measured.<sup>6</sup>

Using such partial PSs for the pulses (but now at both the restricted and full longitude resolutions), we also computed correlation functions that included the longitude ranges of both the MP and IP. These showed no significant ( $>3$  standard deviations in the off-pulse noise) level of correlation at lags of either 0 or  $\pm 1$  pulse.

We also computed partial profiles for the null partial PSs, having lengths of 4635 and 3667 at P and L band, respectively. In these, we were able to find neither significant total power nor any correlated PPAs that might indicate weak linear polarization in the baseline regions. This circumstance argues very strongly that the IP either nulls, or remains very inactive, during MP nulls.

#### 4 EMISSION GEOMETRY OF THE MAIN PULSE AND INTERPULSE

At various stages of our analyses we had indications that the baseline regions of the full period profiles were significantly linearly polarized. In order to explore this further, we reprocessed our observations in a manner such that no baseline level was subtracted from Stokes  $Q$  and  $U$ . We then found a significant level of linear polarization in both regions between the MP and IP corresponding to some 0.25% of the MP peak at P and 0.8% at L band. In both cases the PPAs associated with this baseline linear polarization are nearly flat, suggesting that only one Stokes parameter is well defined, therefore we have concluded that this baseline polarization cannot be well measured with our polarimeter configurations.<sup>7</sup> Again, we stress that this baseline linear power is associated with the pulses and not the nulls! HF86 also allude to a “bridge” of total power emission between the star’s MP and IP (see their fig. 2d and the associated discussion).

Regardless of whether the star is classified as a member of the  $cT$  or  $cQ$  class, it can be said with confidence that our sightline crosses two concentric emission cones. The weaker cone is encountered on the profile edges and exhibits similar properties and dimensions at the two frequencies. It is the stronger central emission that shows an “unresolved double” pattern above 1 GHz and a more “single” form at

<sup>6</sup> Thanks to Tim Hankins, we have been able to examine the interpulse-discovery observations that were reported in HF86, and we can see how their interpretation of a frequency-dependent  $\Delta\phi_{IP-MP}$  arose. At that time, it could not have been realized that the unusual shape changes of B1944+17’s MP make it nearly impossible to correctly align profiles of different frequencies.

<sup>7</sup> The L-band system consists of dual linears and the P band dual linears with a circular hybrid between the feed and the cal injection; thus in neither system are Stokes parameters  $Q$  and  $U$  determined fully by correlation of the receiver voltages.

meter wavelengths. Two aspects of this profile’s evolution are quite unusual (*e.g.*, R93a,b): a) that the central emission pattern narrows (shows a smaller equivalent width) at lower frequencies, and b) that the “outriding” component pair retains essentially the same dimensions between the two bands. Generally, we encounter outer cones on profile edges, and these show substantial “spreading” with wavelength; whereas inner cones are seen inside the outer ones and show little spectral variation in their dimensions. In B1944+17 these usual expectations seem reversed; how could this occur?

#### 4.1 Assembling the Relevant Evidence

Careful reference to the total power profiles of Fig. 7 shows that the MP and IP are both rather broad—as is expected for a small value of  $\alpha$ —with emission extending over most or all of  $60^\circ$  in each case. Moreover, (HF86 notwithstanding), the MP to IP spacing is close to half the rotation period. Given the complex and changing form of the MP in particular, it is difficult to be more precise than this.

Several aspects of the linear polarization are also important to note: First, the absolute PPAs associated with the central longitudes of the MP and IP are nearly identical—allowing for the  $90^\circ$  OPM “jumps”—arguing that the respective emission regions are either conjunct or in opposition along a given magnetic longitude. Second, the PPA traverses under the MP and IP have opposite senses. At both frequencies,  $90^\circ$  OPM-dominance “jumps” occur on both the leading and trailing edges of the **MP** profiles.

Third (see Fig. 1), the MP PPA traverse is unusually shallow. Its sweep rate  $R$  ( $= \Delta\chi/\Delta\phi$ ) is only some  $\pm 0.75^\circ/^\circ$  and remarkably linear across the bodies of both the P and L-band profiles. The shallow PPA traverse indicates that the magnetic colatitude  $\alpha$  and sightline-impact angle  $\beta$  are similar and both small (*i.e.*, the sweep rate  $|R| = \sin\alpha/\sin\beta$ ). Interestingly, the negative sweep rate of the IP has an even shallower slope.

Finally, the interpulse emission is of an entirely different character than that of the MP. The MP has a complex structure of regions with different dynamics and OPM activity, whereas the IP is more nearly unimodal in form (though with low persistent peaks) and fully linearly polarized. In contrast to the MP, it displays a continuous, smooth PPA traverse—*i.e.*, it does not show any “ $90^\circ$  jumps” as the MP does. Moreover, the IP emission seems uncorrelated with that of the MP. These MP and IP properties provide crucial information about the emission geometry as we will see below.

#### 4.2 Building A Geometrical Model

While B1944+17’s IP has been known for more than 20 years (HF86), its polarization properties are measured here for the first time. Therefore, all previous efforts to understand the star’s basic geometry have been based on its MP properties alone. HF86 speculated about whether the IP reflected a single or two-pole configuration, but made no attempt at a quantitative model. The star’s unusually shallow  $R$  value presents a major difficulty for any model. Indeed, the only published model (R93a,b) views the pulsar’s MP

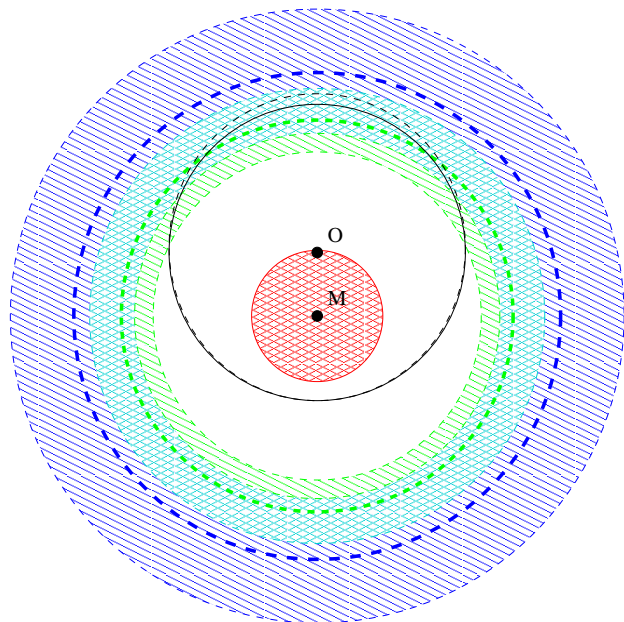


**Figure 8.** Diagram showing the apparent sightline geometry of pulsar B1944+17. The outer cone is shown in blue, the inner cone in green, and their overlap region in cyan. The core beam is then shown in red. The radial peaks of the respective cones are shown by thick blue and green dashed lines. The edges of the beams show their half power points (see text). The magnetic axis is marked with an “M” and the rotation axis with an “O”. As we know little for B1944+17 about the frequency dependence of the beam dimensions, we have used their (R93a,b) nominal 1-GHz values—*e.g.*,  $8.7^\circ$  for the outer beam’s outer 3-dB radius (see text). The observer’s sightline orbit then makes a small circle around the rotation axis such that it touches both cones and the periphery of the core beam. The beam pattern has a larger angular size at the lower frequency, so we show the *relative* size of the sightline orbit within the beam pattern. The L and P-band sightline orbits

are then indicated by dashed and solid black curves, respectively.

profile as **cT** and obtains reasonable dimensions for the inner and outer cones—but only by assuming that the apparent  $R$  value was somehow too flat. The actual sweep rate of  $0.75^\circ/^\circ$  implies that  $\alpha$  will be even smaller than  $\beta$ . This also suggests strongly that the observer’s sightline to B1944+17 largely remains inside its emission cones! A current PPA fit to our same 327-MHz observations that includes the IP (Mitra & Rankin 2010; see their fig. A8) gives highly correlated (98%)  $\alpha$  and  $\beta$  values of  $2.8$  and  $4.0^\circ$ , respectively, with large errors ( $\pm 15^\circ$ ). Clearly, somewhat different values of  $\alpha$  and  $\beta$  that maintained  $R$  would also fit the PPA traverse well.

The half- or equivalent widths of the MP and IP are roughly equal and occupy opposing  $\sim 60^\circ$  or  $1/6$  sections of the star’s rotation cycle. Moreover, the similar PPA ranges and opposite slopes of the MP and IP traverses argue that our sightline cuts these regions within the same range of magnetic longitude (modulo  $180^\circ$ ) but at different colatitudes. This symmetry is consistent both with an orthogonal rotator model (in which the MP and IP emission comes from the two respective poles) as well as a single pole model (wherein both MP and IP are emitted within a single polar region). Notably, the extreme shallowness of  $R$  and the

small values of  $\alpha$  and  $\beta$  are more consistent with the latter configuration.

The very small  $\alpha$  and  $\beta$  values indicate that the pulsar is a nearly aligned rotator with the Earth positioned almost directly above its “nearer” polar cap of emission, similar to the single pole IP model first proposed by Gil in 1985. According to this model, the MP is a result of our sightline first crossing the inner cone of emission obliquely, then making a tangential cut through the inner/outer cone overlap region, and finally recrossing the inner cone symmetrically. Such an “inside out” sightline traverse accounts for the stability of the outer parts of the MP profile as well as the unusual frequency dependence of the middle region. Moreover, the weak IP feature can apparently be understood as a grazing encounter of the sightline with the far “skirts” of the core beam—such that the MP and IP are centered on opposing field lines that are cut in the same directions.

Finally, we can assemble the elements of a quantitative model for the emission geometry of B1944+17. Following R93a,b we know that the outer and inner conal beams have particular dimensions at 1 GHz, here specified in terms of the outside half-power points (which for a 440-ms pulsar) are  $8.7^\circ (=5.75^\circ P_1^{-1/2})$  and  $6.5^\circ (=4.33^\circ P_1^{-1/2})$ , respectively. A similar model is available for the peaks of conal beams (Gil *et al.* 1993) such that these fall at  $6.9^\circ (=4.6^\circ P_1^{-1/2})$  and  $5.6^\circ (=3.7^\circ P_1^{-1/2})$ . No such study has determined the inner half-power dimensions of conal beams, but if we assume that they are radially symmetric, we can estimate their inner dimensions from the above data. These values are then  $5.2^\circ (=3.45^\circ P_1^{-1/2})$  and  $4.5^\circ (=2.97^\circ P_1^{-1/2})$  as above, respectively. These conal beam characteristics are illustrated in Figure 8: the outer and inner cones are hashed in blue and green, respectively, up to their half-power levels, and their peaks are indicated by heavy colored dashed lines. Note that the two beams overlap significantly (as they often do in actual profiles) and this overlap region is hashed in cyan. Finally, the core beam is shown in red hashing centered on the magnetic axis (“M”) out to its  $1.8^\circ (=2.45/2P_1^{1/2})$  half-power point.

The respective L (**dashed**) and P (**solid**) sightline trajectories are then fitted into the above radiation-beam geometry as indicated in Fig. 8 by the black sightline curves centered on the rotation axis (“O”). **The magnetic colatitude  $\alpha$  is about  $1.8^\circ$ , the sightline impact angle  $\beta$  about  $2.4^\circ$ , making the sightline circle radius just over  $4^\circ$ .** Of course, the angular radius of the sightline circle does not vary with frequency. Given, however, that the B1944+17 profiles provide very little information about the “conal spreading” at meter wavelengths, we have chosen to illustrate the pulsar’s geometry using the well determined 1-GHz dimensions of the beam structure. In relative terms then, the sightline at L band extends well past the radial maximum point of the **inner** cone, such that it exhibits a cQ structure; whereas the P-band traverse falls just short of this point and has a cT form. In both cases the sightline encounters the core producing the IP.

The multiple lines of evidence that our analyses of this pulsar provide point strongly to the unusual emission geometry discussed above. Were reliable baseline polarimetry available, the sightline traverse could be modeled in considerable detail and the actual dimensions of the several beams

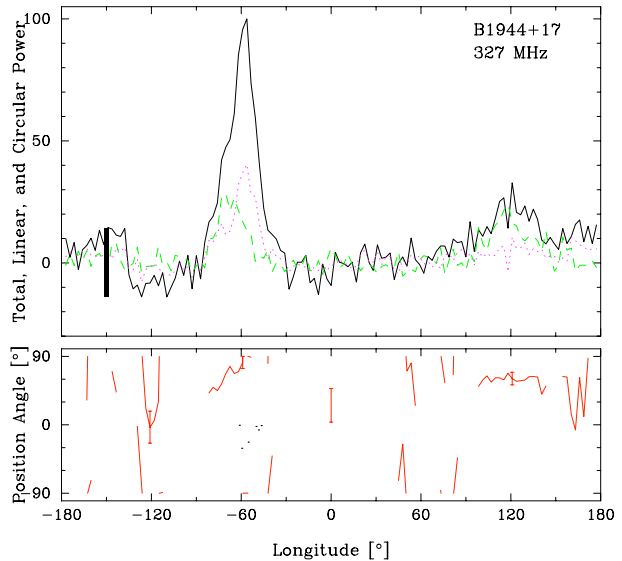


**Figure 9.** The short null profile—*i.e.*, the sum of all 296 P-band pulses which participate in nulls less than 8 periods in length. An intensity threshold of  $0.28 \langle I \rangle$  was used to differentiate between nulls and bursts. Then, those pulses in the short null sequence which still displayed visible power (appeared to possibly be weak bursts) were removed by hand. The remaining weak MP and IP profile corresponds to an intensity threshold of  $0.18 \langle I \rangle$ , and indicates that there is a weak intensity signal (not detectable on a single pulse basis) present in the pulses which participate in short nulls.

estimated through fitting. Unfortunately, this work remains beyond the scope of this paper. Nonetheless, we believe that the circumstances responsible for the B1944+17 interpulse are largely understood—that both the MP and IP are emitted by a single pole and that the IP very likely represents weak core emission.

## 5 HOW CAN WE UNDERSTAND B1944+17’S NULLS?

Pulsar B1944+17 has been most famous for its remarkably long null intervals, which contrast so beautifully with its intense and well organized burst sequences. The star is in the null state some two-thirds of the time, on average. Notably, this value is the same for both the main pulse and the interpulse.

Since Backer’s first documentation of pulsar nulling in 1970, the principal question surrounding nulls has been one of causality. Here we discuss and distinguish between nulls that are likely caused by two entirely different mechanisms: empty sightline traverses across a rotating carousel, and cessations of emission. We find that the two null mechanisms can largely be distinguished by their characteristic lengths, and we will therefore refer to them as such: the former being short nulls ( $\lesssim 7 P_1$ ), and the latter long ones ( $\ll 7 P_1$ ). Note that this  $7 P_1$  boundary falls on the tail end of the random distribution of null lengths in Fig. 2, whereas the long nulls quickly become non-random.

## 5.1 Null Analysis

It is important to note that the distinction between short and long nulls is not a clear one. In this investigation, the numerical boundary was set by averaging the total power in a series of null sequences, with varying upper bounds in null length, then selecting the short versus long null boundary to be where the average power dropped off. This procedure makes no claim of being exact. We are primarily interested in the possibility that B1944+17 exhibits two distinct types of nulls, rather than in defining their features precisely.

### 5.1.1 Short Nulls

Short nulls can be found in virtually any context of this star’s emission—that is, they are not unique to a particular mode, nor do they only occur between mode changes. The short null average profile was constructed by summing all the nulls (falling below the established threshold,  $0.28 \langle I \rangle$  at P band) which participated in null sequences  $\leq 7 P_1$  in length (after removing a few with obvious “burst” power by hand). The total power in the short null average profile in Figure 9 (comprised of the 296 remaining nulls) was nonzero—*i.e.*, it did **not** represent noise, rather there is very clear indication of emission. This short null profile—showing clear emission features at the positions of the MP and IP—exhibits an aggregate intensity  $0.18 \langle I \rangle$ , a level well below the threshold but far above the noise fluctuations.

It is challenging yet of great importance to decipher whether this non-zero power is the result of emission from (a) consistent low intensity emission throughout the null sequences and/or (b) a small number of high-*er* intensity pulses that skew the average. To reduce the possibility that the detected profile was due to (b), we reemphasize, the few pulses (**half a dozen**) for which there was visible power (*i.e.*, perhaps “should” have been called weak bursts) were removed by hand from the short null partial PS. It was then after this procedure that significant power was detected in the short null profile (whereas, we will see below that the long null profile is indistinguishable from noise). We therefore conclude that the power in the short nulls is due to (a): consistent low intensity emission not detectable on a single pulse basis.

Short nulls are more or less randomly distributed throughout the PSs both at L and P band. Recall that B1944+17’s subpulses consistently repeat behaviors (evidenced by the star’s well defined modes) though not with any perceptible regularity. It is not surprising that the short nulls complementing such modes appear consistently, but not periodically.

Mode changes are often, though not always, punctuated by short nulls. Modes A and D are often interrupted by short nulls of some 1–3  $P_1$ . Of the four modes, mode D is most frequently punctuated by short nulls. That the short nulls probably represent empty sightline traverses is very consistent with mode D’s emission behaviors. Mode C characteristically alternates short quasiperiodic bursts and nulls of some 10 – 20  $P_1$ . These transitions between nulls and bursts appear to entail no turnoff as no possible such “partial null” was ever observed in the pulse window. Their characteristic length falls roughly on the boundary where we distinguish between short and long nulls. We have found no

means of testing whether these mode-C nulls represent the longest pseudonulls or the shortest of the long null intervals.

### 5.1.2 Long Nulls

The rest of the story belongs to the long uninterrupted null sequences. As mentioned earlier, B1944+17’s nulls last up to 300  $P_1$  in our observations; however, note that we define long nulls to be any null sequences lasting longer than 7 rotation periods. Long nulls appear very consistently in this pulsar, and their presence alone indicates an “undermixing” of bursts and nulls. As discussed in §3 and displayed in Fig. 3, the long null distribution is highly non-random.

In contrast to the short nulls, the aggregate power in the long nulls at P band is only  $0.009 \langle I \rangle$ , roughly that of noise fluctuations, demonstrating that there is truly no measurable power from the star during these nulls. Every long null interval in our observations has a noise-like profile. This is the case at both L and P band.

Considering their noise-like character, length, and non-random distribution, the probability that long nulls represent “empty” sightline traverses is extremely small. The evidence assembled indicates that long nulls represent actual cessations of the pulsar’s emission. This finding would be strengthened by measuring a decrease in spindown rate during the nulls, as in B1931+24; unfortunately, even the longest nulls in B1944+17 are far too short for this to be possible.

In summary, we find that there are two distinct mechanisms behind B1944+17’s nulls: first, short *pseudonulls* that are an artifact of carousel properties and rotation, exhibit measurable aggregate emission and tend to punctuate high intensity, well structured burst sequences; and second, long (true) nulls which are distributed non-randomly, have no detectable aggregate power, and thus plausibly represent actual cessations of the pulsar’s emission engine. In view of this star’s varied emission behaviors, it is not surprising that its nulling phenomena are similarly complex.

### 5.1.3 Null transitions

Deich *et al.* looked for, but did not observe, transitions from the null-to-burst or burst-to-null state, that were expected to occur infrequently just as the star’s emission cone swept through the Earth’s direction—that is, occasions when the star’s emission switched off or on *during* the pulse window. In our investigation we found two such possible transitions at L band, one from the burst-to-null state and the other the opposite.

In this PS there were some 100 long null intervals, therefore some 200 transitions to and from long nulls. As the MP profile has a roughly  $30^\circ$  equivalent width, we have at best a  $\frac{1}{12}$  chance of observing a given transition. This implies about 17 transitions; however we were able to identify only 2 with good confidence. This seeming shortage of null-burst transitions cannot be read into deeply: a) it may be that such transitions can be securely identified only over a  $10\text{--}15^\circ$  interval, b) a number of the shorter long null intervals may not be what they seem, or c) confident detection may require particular modes before and after the long null. And in any case, merely 2 partial nulls throws any speculation into the regime of small number statistics.

This all said, both transitions occurred approximately halfway through the pulse window and were marked by a sharp decrease or increase in emission intensity. Both transitions occurred on the edges of long null intervals, from mode C in both cases. If these are valid indicators of transitions to or from cessations of emission, they occur on millisecond scales that are comparable to our longitude resolution.

## 6 SUMMARY AND DISCUSSION

We have thoroughly investigated the radio pulse-sequence properties of pulsar B1944+17. This star nulls some two-thirds of the time, has four distinct modes of emission and an IP, and we find that its magnetic and rotation axes are closely aligned.

We confirmed the four modes first identified by Deich *et al.*. Their properties are as follows:

- Mode A is the brightest and most ordered of the star’s four modes. It consistently displays three to four subpulses that drift with a  $P_3$  value of about 14 periods.
- Mode B drifts at a faster rate and displays a  $P_3$  of approximately 6  $P_1$ . It usually shows three subpulses, which are characteristically less ordered than those of mode A.
- Mode C resembles mode A but is stationary. It displays between one and three subpulses with similar brightness and virtually identical spacing ( $P_2$ ) to those of mode A, however with negligible subpulse drift—and bursts alternate quasiperiodically with nulls of 10-30  $P_1$ . Mode C may be interpreted as representing a carousel of “beamlets” organized in the same way as in mode A, but which is nearly stationary and flickering quasiperiodically.
- Mode D is the weakest of the four modes. Though it lacks the ordered drift bands of the other modes, we find that it is not chaotic as it had been previously described by DCHR. Its brightest subpulses are in the leading edge of the pulse window, appear consistently at the same phase, and remain active for some 5 periods or so.
- Both the total power and the FWHM as displayed in the modal average profiles show consistent behaviors *within* the different modes.

In order to provide a sound basis for interpretation, we investigated B1944+17’s emission geometry, and we drew the following conclusions:

- The pulsar has both an MP and IP, which occupy opposing roughly  $60^\circ$  intervals of its rotation cycle.
- The MP and IP are separated by almost exactly half a rotation period, independent of radio frequency.
- The nearly complete linear polarization and disorderly PS modulation of the IP stands in stark contrast to the modest linear and rich phenomenology of the MP.
- The IP subpulses vary widely in intensity but show negligible correlation with subpulses in the MP.
- The MP’s equivalent width increases with increasing frequency, whereas its full width is nearly constant over a broad band. This appears contrary to the frequency evolution exhibited by most other pulsars.
- The PPA rates ( $R$ ) of the star’s MP and IP are unusually small, but of opposite senses. The MP value is only  $+0.75^\circ/^\circ$ .

- Emission-beam modeling constrained by the MP and IP PPA-traverse information argues that  $\alpha$  and  $\beta$  are some  $1.8$  and  $2.4^\circ$ , respectively—such that the sightline orbit has an angular radius of just over  $4^\circ$  and remains inside the conal emission beam (See Fig. 8).

- The small  $\alpha$  and  $\beta$  values indicate an unusual single-pole interpulse geometry—that is, here the IP emission occurs along field lines opposite to the MP and is produced by weak core emission.

- The rarity of B1944+17’s geometrical configuration seems to account for some of its perplexing modulation and polarization phenomena.

The prominent nulls of pulsar B1944+17 have been the principal interest driving this investigation. Here, we summarize the patterns of its nulling behavior, discuss the null-length distribution, and evaluate which possible mechanisms are responsible for the nulls.

- B1944+17 appears to null nearly 70% of the time. That is, some two-thirds of the star’s “pulses” have intensities falling below a plausible “null threshold” and are putative nulls. In practical terms then, there is a two-thirds chance that any given “pulse” will be a “null” rather than a burst.

- In the above context, it is remarkable to find that B1944+17 exhibits bursts lasting up to 100 or so  $P_1$  and nulls with durations of up to some 300 periods.

- In Runs Test terms, the star’s long nulls and bursts are non-randomly “undermixed”.

- One-period nulls appear with the highest frequency. Nulls with lengths up to approximately 7  $P_1$  or so occur with a roughly random distribution; whereas nulls longer than this are obviously (and increasingly) non-random.

- The short nulls—that is, those with durations less than roughly 8  $P_1$ —have significant aggregate power in the form of a weak average MP and IP profile; see Fig. 9. These short nulls are largely *pseudonulls*—that is, “empty” sightline traverses through the rotating carousel-beam system.

- Nulls longer than the above, on the other hand, exhibit negligible aggregate power and thus have the character of noise. These long nulls then represent actual cessations of the pulsar’s emission. B1944+17’s behavior is therefore similar to the intermittent pulsar B1931+24 (Kramer *et al.* (2006)).

On this basis, we can draw some interesting conclusions about the overall emission properties of pulsar B1944+17—

- Within certain A- or B-mode PSs, the emission from the pulsar’s inner and outer cones exhibits similar modulation frequencies and thus folds synchronously. This strongly suggests that the inner and outer-cone emission is produced by the same set of particles.

- Similarly, the MP and IP emission generally bursts and nulls together, but is otherwise uncorrelated. This suggests either that the core emission is produced at low altitude within the polar flux tube by sets of particles that produce the conal emission at higher altitude, or, perhaps that the conal emission is refracted inward as suggested by Petrova & Lyubaski (2000).

- If we are correct about the star’s emission geometry, then the star’s subpulse modulation reflects a complex combination of inner and outer-cone contributions.

Our analyses found no basis for determining the pulsar’s carousel circulation time; however, some speculations are appropriate. First, identification of a circulation time may be difficult or impossible in a pulsar with intermittent emission. Second, rough estimations of the star’s circulation time from Ruderman & Sutherland (1975) or by extrapolating from B0943+10 (DR01) both suggest that it could be short—*i.e.*, 10-15  $P_1$ . If there were then 10 or more “beamlets” in the carousel, the primary “drift” modulation frequency could be aliased into the second order. Such aliasing together with discrete changes in “beamlet” number could give rise to “modes” such as are observed in B1944+17. For instance, were the star’s carousel to circulate in some 12  $P_1$  with a configuration of 13 “beamlets”, drift modulation similar to the A mode would be produced. Similarly, 14 “beamlets” would modulate the PSs with a  $P_3$  like that of the B mode, and 12 would produce a nearly stationary modulation very like that of mode C.

We found it both fascinating and challenging to study a star such as B1944+17 which exhibits so many distinct phenomena. Clearly, its complex modes and nulls still have much to teach us. Different polarization measurements may be able to better define its sightline geometry, and interferometry could well reveal a “pedestal” of continuous emission. Finally, even longer observations are needed to further explore the star’s carousel-beam configuration and fully assess the frequency of partial nulls.

## ACKNOWLEDGMENTS

We are pleased to acknowledge Vishal Gajjar, Tim Hankins, Joeri van Leeuwen and Geoffrey Wright for their critical readings of the manuscript and Jeffrey Herfindal for assistance with aspects of the analysis. We also sincerely thank both Tim Hankins for providing us with the original interpulse discovery observations, and Joel Weisberg for the ionospheric Faraday rotation corrections. One of us (IMK) sincerely thanks the Barry M. Goldwater Scholarship and Excellence in Education program and the UVM College of Arts and Sciences for the APLE Summer Fellowship, which together permitted her to complete this work. The other (JMR) thanks the Anton Pannekoek Astronomical Institute of the University of Amsterdam for their generous hospitality and the Netherlands National Science Foundation and ASTRON for her Visitor Grants. Portions of this work were carried out with support from US National Science Foundation Grants AST 99-87654 and 08-07691. Arecibo Observatory is operated by Cornell University under contract to the US NSF. This work used the NASA ADS system.

## REFERENCES

Backer, D. C. 1970 *Nature*, 228, 1297  
 Deshpande, A.A. & Rankin, J.M. 1999, *Ap.J.*, 524, 1008  
 Deshpande, A.A., Rankin, J.M., 2001, *MNRAS*, 322, 438  
 Deich, W. T. S., Cordes, J.M., Hankins, T.H., & Rankin, J.M., 1986 *Ap.J.* 300, 540  
 Gil, J. 1985 *Ap.J.*, 299, 154  
 Gil, J.A., Kijak, J., & Seiradakis, J.H. 1993, *A&A*, 272, 268  
 Hankins, T. H. & Fowler, L. A. 1985, *Ap.J.*, 304, 256  
 Herfindal, J. L., & Rankin, J. M., 2007, *MNRAS*, 380, 430

Herfindal, J. L., & Rankin, J. M., 2009, *MNRAS*, 393, 1391  
 Hobbs, G., Lorimer, D. R., Lyne, A. G., & Kramer, M. 2005, *MNRAS*, 360, 974  
 Johnston, S., Hobbs, G., Vigeland, S., Kramer, M., Weisberg, J. M., & Lyne, A. G. 2006, *MNRAS*, 364, 1397  
 Keith, M. J., Johnston, S., Weltevrede, P., & Kramer, M. 2010, *MNRAS*, 402, 745  
 Kramer, M., Lyne, A. G., O’Brien, J. T., Jordan, C. A., & Lorimer, D. R. 2006, *Science*, 312, 549  
 Lyne, A.G., & Manchester, R.N. 1988, *M.N.R.A.S.*, 234, 477  
 Mitra, D., & Rankin, J. M. 2010, *Ap.J.*, submitted  
 Petrova, S. A., & Lyubarskii, Y. E. 2000, *A&A*, 355, 1168  
**Rankin, J.M., 1986, *Ap.J.*, 301, 901**  
 Rankin, J.M., 1993a, *Ap.J.*, 405, 285  
 Rankin, J.M., 1993b, *Ap.J. Suppl.*, 85, 145  
 Rankin, J.M., 2007, *Ap.J.*, 664, 443  
 Rankin, J. M. & Wright, G.A.E. 2007, *MNRAS*, 379, 507  
 Rankin, J. M. & Wright, G.A.E. 2008, *MNRAS*, 385, 1923  
 Redman, S. R., Wright, G.A.E., & Rankin, J. M., 2005, *MNRAS*, 357, 859  
 Redman, S. R., & Rankin, J. M., 2009, *MNRAS*, 395, 1529  
 Ruderman, M., & Sutherland, P. 1975, *Ap.J.*, 196, 51  
 Suleymanova, S. A., & Rankin, J. M. & 2009, *MNRAS*, 396, 870  
 Weltevrede, P., Edwards, R. T., & Stappers, B. W. 2006, *A&A*, 445, 243  
 Weltevrede, P., Stappers, B. W., & Edwards, R. T. 2007, *A&A*, 469, 607  
 Weltevrede, P., & Wright, G.A.E. 2009, *MNRAS*, 395, 2117